Supplementary Materials for

A Self-Sufficient Biocatalytic Photo-Fenton System Using Immobilized Glucose Oxidase

Authors

Shifei Kang,[1,†] Chenjun Lei,[1,†] Chenjie Ding,[1,†] Lasse Hyldgaard Klausen,[2]

Bianxiao Cui,[3,*] Lifeng Cui[4,*]

Affiliations

1. Department of Environmental Science and Engineering, University of Shanghai for Science and Technology, Shanghai 200093, China.

2. Interdisciplinary Nanoscience Center (iNANO), Sino-Danish Center for Education and Research, Aarhus University, DK-8000, Aarhus C, Denmark

3. Department of Chemistry, Stanford University, Stanford, California 94305, United States.

4. College of Smart Energy, Shanghai Jiao Tong University, Shanghai 200240, China

† These authors contributed equally to this work
* **Correspondence: bcui@stanford.edu** (BC), **lifeng.cui@gmail.com** (LC)

This file includes:

Supplementary note 1: Characterization of materials

X-ray diffractometer (XRD) patterns were recorded on a Bruker D8 Advance instrument under Cu Kα radiation at emission current of 40 mA and accelerating voltage of 40 kV. The Thermo ESCALAB 250 X-ray photoelectron spectroscope (XPS) was run under Al Kα monochromatization. The JEM-2100F transmission electron microscope (TEM) was operated at an accelerating voltage of 200 kV. The Brunauer-Emmett-Teller (BET) specific surface area (S_{BET}) and pore structure of the materials were detected on a nitrogen adsorption-desorption instrument (Quantachrome autosorb-iQ-2MP). UV-Vis diffuse reflectance spectra (DRS) were obtained under a Shimadzu UV-2600 spectrometer. Electrochemical measurements were performed on a CHI600C electrochemical workstation. The Fourier transform infrared (FT-IR) spectroscopy on KBr pellets of the materials was collected by a Thermo Scientific Nicolet iS50 FTIR spectrometer. Electrochemical impedance spectroscopy (EIS) and transient photocurrents were recorded by a Chi660e electrochemical workstation based on a conventional three-electrode system from frequency 0.01 Hz to 100 kHz at the circuit potential. Photoluminescence (PL) spectra were observed by a Hitachi F-7000 fluorescence spectrophotometer under excitation at 367 nm. Magnetic properties were determined by a vibrating sample magnetometer (VSM, 7404, LakeShore, USA). Elemental analysis of iron content was conducted by using an Agilent ICP-OES 730 instrument. Electron paramagnetic resonance (EPR) measurements were performed on a Bruker EPR A300 spectrometer equipped with a 300 W xenon lamp. EPR signals captured by DMPO were detected in different air saturated methanol / water dispersions of corresponding samples with and without glucose.

Supplementary note 2: Photocatalytic activity evaluation

Photocatalytic activity of each sample was preliminarily measured by detecting the effect of tetracycline and dye degradation in an aqueous suspension in a quartz tube. In the photo-Fenton experiment, 50 ml tetracycline (initial 20 mg/L) and Rhodamine B dye (initial 10 mg/L) were placed in a quartz reactor, and 25 mg of a catalyst was added in the solution. The mixture was put into the reactor dark reaction firstly to ensure the adsorption-desorption equilibrium between the catalyst and the pollutants. The reaction was then initiated by adding 0.25 mL of H_2O_2 (30 wt%) and simultaneously turning on visible light. The average light irradiation intensity was powered by a 500 W Xe lamp with a 420 nm optical filter. For the dark Fenton reaction, the amounts of the catalyst and reagent were the same as above, except for the lack of exposure to visible light. The reaction temperature was maintained at 25 °C by a circulating water bath cooling. At pre-determined time interval, 2 mL of the suspension was extracted and filtered to obtain the supernatant for testing. The sample solutions were filtered with Millipore filter (pore size: 0.22 μm), and then monitor the absorbance of the solution at 357 nm and 554 nm with an Evolution Thermo 600 UV-vis spectrophotometer to determine the residual concentration of tetracycline and rhodamine B dyes, respectively. For Fe-g-C_3N_4/GOD system, the amount of catalyst and reagent is

the same as above, but the addition of 0.25 mL of H_2O_2 (30 wt%) is replaced by 0.6g β-D-glucose. For the repeated reactions, the catalyst after the reaction was washed with deionized water for several times and then dried. The reaction conditions were the same as before.

The absorbance of the tetracycline solution and rhodamine B dye was detected by 600UV-vis spectrophotometry at 357 nm and 554 nm, respectively. The pollutants removal efficiency was calculated as follows:

$$Degradation\ efficiency\ (\%) = \frac{C_0 - C}{C_0} \times 100\#(1)$$

where C_0 and C are the pollutants concentrations initially and after given time of irradiation, respectively.

The COD was measured via titration with potassium dichromate. The sample was centrifuged to remove the catalyst and then 10 ml was removed and placed in an Erlenmeyer flask. Next, 5 ml of 0.25 M potassium dichromate and 15 mL of sulfuric acid were added. This was refluxed for 2 h and then cooled after adding 45 ml distilled water to rinse the condenser tube. Then added three drops of ferrioxide indicator and titrated it with 0.05 M ferrous ammonium sulfate solution. The color changed from yellow to blue-green and finally to red brown. This is the endpoint of the titration; the COD was calculated according to the formula. (Each experiment had a blank that used 10 ml distilled water instead of water sample with other steps remaining the same.)

In this formula:

$$\rho = \frac{C \times (V_0 - V_1) \times 8000}{V_2}\#(2)$$

C: Ammonium ferrous sulfate standard solution concentration

V_0: Blank sample consumption volume of ammonium ferrous sulfate

standard solution, ml

V_1: Determination of the volume of ammonium ferrous sulfate

standard solution consumed in water samples, ml

V_2: Sample volume, ml

The biochemical oxygen demand (BOD) of a given water sample is measured using the conventional BOD_5 measurement method. BOD is typically measured using a conventional BOD_5 assay, which is a five-day incubation of initially air-saturated, diluted aliquots of the sample with mixed communities of bacteria. Since the amount of glucose added in the experiment is limited (less than 10 mg/L), and glucose is easily biochemically processed and can even be used as a carbon source in biological process, our experimental results are calculated and displayed after deducting the influence of glucose.

Supplementary note 3: Detection of generated H_2O_2

The concentration of H_2O_2 in the reaction system was quantitatively analyzed using a commercial hydrogen peroxide (H_2O_2) detection kit based on the titanium sulfate method. In this assay, H_2O_2 reacts with titanium sulfate to form a yellow pertitanium complex, which exhibits a characteristic absorption peak at 415 nm. At designated time intervals, 100 μL of the reaction suspension was extracted from the reactor and immediately filtered through a 0.22 μm syringe filter to remove catalyst particles. Subsequently, the filtrate underwent a colorimetric reaction according to the manufacturer's protocol. The absorbance of the resulting solution at 415 nm was determined using a UV-vis spectrophotometer. The H_2O_2 concentrations measured are summarized in Table S1.

Supplementary note 4: Detection of Fe^{2+} and Fe^{3+}

Following the reaction, the supernatant was pretreated by microwave digestion, and the total iron concentration was determined to be 276.708 μg/L by ICP-OES. The dissolved ferrous ions and total iron ions were quantified by the 1, 10-phenanthrolin method and analyzed by at maximum wavelength of 510 nm with a UV–vis spectrophotometer (UV-2600 spectrometer, Shimadzu, Japan). The total iron ion was measured with addition of hydroxylamine hydrochloride. The content of trivalent iron can be obtained by the difference between total iron and ferrous ion.

Supplementary note 5: Recovery by magnetic separation.

Following the r photo-Fenton reaction, the catalyst suspension was collected in a 50 mL centrifuge tube. The magnetic catalyst was then separated from the solution by placing a strong NdFeB magnet against the exterior of the tube. After approximately 2 minutes, the clear supernatant was carefully decanted. To wash the catalyst, the magnet was removed, 20 mL of deionized water was added, and the particles were thoroughly redispersed via vortexing. This magnetic separation-washing cycle was repeated three times to remove any residual species from the catalyst surface.

The finally recovered catalyst was transferred to a pre-weighed watch glass, dried to a constant weight in a vacuum oven at 60 °C, and then cooled to room temperature in a desiccator. The catalyst recovery rate was calculated using the following equation:

$$R = \left(\frac{m_2}{m_1}\right) x100\% \quad \#(3)$$

M_1: The initial mass of the catalyst

M_2: The final mass of the dried, recovered catalyst.

Supplementary note 6: Photo-Fenton activity and physiochemical characterizations of Fe-g-C_3N_4 catalysts and Fe-g-C_3N_4/GOD catalysts.

Melamine and $K_4Fe(CN)_6 \cdot 3H_2O$ were put into a covered crucible, which was then heated at a rate of 5 °C•min^{-1} to 550 °C in a muffle furnace for 4 hours. After that, the crucible was naturally cooled to room temperature. The resulting mixture was ground to powder for further use. (x% Fe-g-C_3N_4). The Fe content in the mixture was prepared at different element mass ratios: 1%, 3%, 5% Fe-g-C_3N_4.The screening photo-Fenton reaction test showed (Fig.S1a) that the Fe-g-C_3N_4 materials are all typical photo-Fenton catalysts, and a remarkable high removal efficiency up to 99% was recorded when the iron content was 3 wt.%. It should be noted that a synergetic effect occurred between Fe-g-C_3N_4 and H_2O_2 under simulated sunlight irradiation, and the Fe^{3+}/Fe^{2+} cycle was boosted by photoelectrons, this is similar with many previous reports on photo-Fenton system. Through the analysis and discussion of the above results, we consider 3%Fe-g-C_3N_4 to display a strong intrinsic photo-Fenton performance and it was thus selected for further experiments with GOD loading and was denoted as Fe-g-C_3N_4.

The chemical structure and surface stoichiometry of the involved elements were investigated via X-ray photoelectron spectroscope (XPS). Fig. S2a shows the full spectrum of all the elements in g-C_3N_4 and Fe-g-C_3N_4. In addition to the peaks of C, N, O found in g-C_3N_4, the XPS spectrum of Fe-g-C_3N_4 also shows the weak peak of Fe. The presence of Fe species in Fe-g-C_3N_4 can be further confirmed by ICP-OES. The XPS C1 s spectrum of g-C_3N_4 can be deconvolved into two peaks at binding energy of 284.8 and 288.1 eV respectively (Fig. S2b), which are ascribed to sp^2 C and ri-s-triazine (heptazine) structures of N-C=N. The XPS N1 s spectrum of g-C_3N_4 can be deconvolved into three peaks with binding energy of 398.9, 399.5 and 400.9 eV respectively (Fig. S2c), ascribed to the sp^2 structure of N (C=N-C), tertiary N- $(C)_3$ and -NH_2 or =NH, as well as a peak at 404.9 eV ascribed to the charge effect. Except for the surface adsorbed water related peaks, the O 1s spectrum exhibits a characteristic peak at 530.3 eV (Fig. S2d), which can be ascribed to Fe-O, indicating the presence of iron oxide species. To confirm the successful immobilization of glucose oxidase (GOx), further XPS analysis was conducted on the Fe-g-C_3N_4/GOD composite. The high-resolution spectra provide compelling evidence for the enzyme loading. Fig. S3a shows the full spectrum of all the elements in Fe-g-C_3N_4/GOD. The C 1s spectrum (Fig. S3b), in addition to the N–C=N peak from the substrate, exhibits new signals at 284.8 eV and 286.3 eV, which are attributed to the C–C/C–H and C–O bonds from the enzyme molecules, respectively. Critically, the N 1s spectrum (Fig. S3c) displays a prominent new peak at 400.1 eV, which is unambiguously assigned to the characteristic amide/peptide bonds (N–C=O) of the protein backbone, serving as a direct signature of the enzyme's presence. This conclusion is further corroborated by the O 1s spectrum (Fig. S3d), where a new peak located at 531.5 eV corresponds to the carbonyl group (C=O) in the peptide bonds. The appearance of these new signals, originating from the characteristic functional groups of the GOx

protein, provides strong evidence for the successful immobilization of the enzyme onto the Fe-g-C_3N_4 support.

After the optimization of pore structure, according to the pore size distribution curve shown in Fig. S4a, both Fe-g-C_3N_4 and Fe-g-C_3N_4/GOD obtained very ideal ~20 nm pore, which is very important for the mass transfer process related to enzyme immobilization and enzyme catalysis. The greatly enhancement of the ideal ~20 nm mesopores are more intuitively presented in the contribution charts of pore volume and specific surface area (Fig. S4b, c).

The XRD patterns of g-C_3N_4-based photocatalysts are typical of two pronounced peaks at 27.5° and 13.1° (Fig. S5a), indexed as the characteristic (002) peak for interlayer stacking of aromatic systems, and the (100) peak corresponding to the interplanar separation respectively. As the Fe content in g-C_3N_4 increases, the intensity of the peaks at the (100) and (002) planes is gradually weakened. The crystallinity of the (100) and (002) crystal planes decreases because Fe affects the thermal condensation of melamine. This phenomenon indicates the inhibitory effects of Fe species on polymeric condensation and host–guest interactions. Furthermore, other characteristic Fe species peaks were not found, which may be due to the limited amount of doped iron.

Fig. S5b illustrates the FTIR spectra of g-C_3N_4 and x% Fe-g-C_3N_4 in the range of 500–4000 cm^{-1}. Pure g-C_3N_4 has three sets of absorption peaks. The peak at 2168 cm^{-1} corresponds to the stretching vibration of CN, which the vibration intensity is enhanced with the increasing Fe content. The broad peak at 3000–3500 cm^{-1} is caused by OH breathing vibration and the stretching vibrations of the terminal $–NH_2$ or –NH located at the defect sites of aromatic rings. The peak at 3180 cm^{-1} corresponds to the N-H stretching vibration, indicating that amino groups are still present in g-C_3N_4 formed by polycondensation of melamine. The absorption peaks at 1200−1700 cm^{-1} are assigned to the typical stretching modes of aromatic carbon nitride heterocycles. The band at 810 cm^{-1} is the characteristic breathing mode of s-thiazine units. All these peaks were also observed in Fe-g-C_3N_4. The peaks did not shift with different amounts of Fe adjunction into g-C_3N_4, but the corresponding peaks did gradually weaken. These results imply that Fe does not change the skeletal structure of g-C_3N_4.

As can be seen from figure S5, the g-C_3N_4 and Fe-g-C_3N_4 shows strong light absorption from UV to visible light. Pristine g-C_3N_4 showed an apparent absorption edge at about 456 nm. However, with the increase of Fe content, the adsorption edge of Fe-g-C_3N_4 obviously red-shifted from 456 to 478 nm, which was caused by the formation of impurity energy levels due to Fe adjunction. This phenomenon indicates that Fe adjunction can effectively enhance the light-harvesting ability of g-C_3N_4.

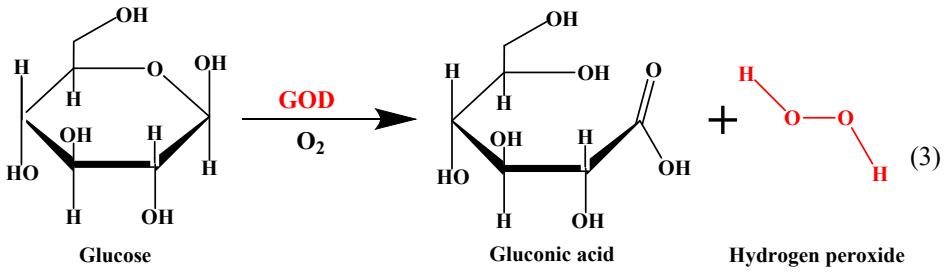

(3)

$$Fe-g-C_3N_4+hv\rightarrow e^-+h^+ \quad (4)$$

$$Fe^{2+}+H_2O_2\rightarrow Fe^{3+}+\cdot OH+OH^- \#(5)$$

$$Fe^{3+}+e^-\rightarrow Fe^{2+}\#(6)$$

$$H^+ +\frac{H_2O}{OH^-}\rightarrow \cdot OH\#(7)$$

$$Fe^{3+}+H_2O_2\rightarrow Fe^{3+}+\cdot OOH+H^+\#(8)$$

$$Fe^{3+}+\cdot OOH\rightarrow Fe^{2+}+O_2+H^+\#(9)$$

$$\cdot OOH\rightarrow \cdot O_2^- +H^+\#(10)$$

$$e^-+O_2\rightarrow \cdot O_2^-\#(11)$$

$$O_2+2e^-+2H^+\rightarrow H_2O_2\#(12)$$

$$e^-+H_2O_2\rightarrow \cdot OH+OH^-\#(13)$$

$$\cdot OH+\cdot O_2^- +Tetracycline\ (dyes)\rightarrow degraded\ products\#(14)$$

Supplementary note 7: Comparison with the conventional Fenton system

For comparison, a conventional Fenton catalyst, FeO_x-g-C_3N_4, was synthesized via a method similar to that for Fe-g-C_3N_4, using ferrous sulfate ($FeSO_4$) as the iron precursor. To initiate the reaction, the same concentration of hydrogen peroxide (H_2O_2) as described above was externally added to the system prior to the photoreaction. The resulting pollutant removal rate was then compared with that of the Fe-g-C_3N_4/GOD/glucose system (Fig.S8).

Supplementary note 8: Evaluation of Anti-interference Capability

To assess the robustness of the Fe-g-C_3N_4/GOD system in a more complex environment simulating real wastewater, a series of anti-interference experiments were conducted.[1] The standard photo-Fenton degradation of tetracycline (TC) was performed with the individual addition of common interfering species: chloride ions (Cl^-), bicarbonate ions (HCO_3^-), and humic acid (HA). Specifically, NaCl (0.1 M), $NaHCO_3$ (10 mM), and humic acid (10 mg/L) were added to the reaction system, respectively. All other experimental conditions, including catalyst dosage, initial TC concentration, glucose concentration, and light irradiation, were kept identical to the standard photocatalytic activity evaluation described in Supplementary note 2. The degradation process was monitored over 120 minutes, and the results are presented in Fig. S9

Table S1: Comparison of Photocatalytic H_2O_2 Production over Different Carbon Nitride Materials

Catalyst	Reaction Time (h)	H_2O_2 Yield (μmol)	H_2O_2 Yield Rate (μmol g^{-1} h^{-1})	Ref.
CN-KI	1	4386.4	4386.4	S[2]
S-CNT	2	59.48	1453.2	S[3]
CN-HP	0.67	4.08	244.8	S[4]
KNiCN	1	3.98	398	S[5]
g-CN-MI-30	30	43.1	14.37	S[6]
Nv–CN	3	5.16	86	S[7]
This work	2	31.7	634	

Table S2: Holistic performance comparison with other advanced Fenton-like systems featuring in situ H_2O_2 generation.

Catalyst System	H_2O_2 Production Rate ($\mu mol\ g^{-1}\ h^{-1}$)	Pollutant & Degradation Efficiency	Catalyst Stability	Consumables/ Energy Input	Ref.
CdS/Fe^{2+}	42.79	45% degradation of Phenol	Not mentioned	Consumable Fe^{2+} (1.8 mM, added each cycle); Pure O_2 bubbling; 300W Xenon lamp	S[8]
Pd0.1/Al	1175	15% removal of Phenol	Ultrasound, 40 kHz, 110 W pH 3.6-9.6	High-energy input (110W Ultrasound)	S[9]
Zn-CNTs/O_2	1550	26.1% removal of SMX	Unstable	Sacrificial metal (Zn^0 consumed). Extreme acidic pH (1.5) required. Pure O_2 bubbling (400 mL/min).	S[10]
Bimetallic Al-Fe/O_2 (Al : Fe=1:1)	Not mentioned	100% removal of 4-Chlorophenol	Unstable	Sacrificial metals (Al^0 & Fe^0 consumed). Extreme acidic pH (2.5) required.	S[11]
Pd_{NP}/CNNT	201.7	Complete inactivation of E. coli was achieved within 5 hours.	Activity declines over 4 cycles	Assumes energy for illumination can be partially offset by savings from reduced mixing/pumping (for pH control) and/or the potential use of solar energy.	S[12]
Cv-PCN	215.44	Not mentioned	minor loss after 10 cycles	HIGHLY ENGINEERED triphase setup required (PTFE-modified foam). Simulated sunlight (100 mW cm^{-2})	S[13]
Co–CeO_2/CeO_2	62.2	Not mentioned	Maintained activity over 5 cycles	Isopropanol (10% v/v, sacrificial agent); Pure O_2 bubbling; 300W Xenon lamp	S[14]
This work	634	60% removal of tracycline	Maintained activity over 4 cycles	Waste saccharides 500W Xenon lamp	

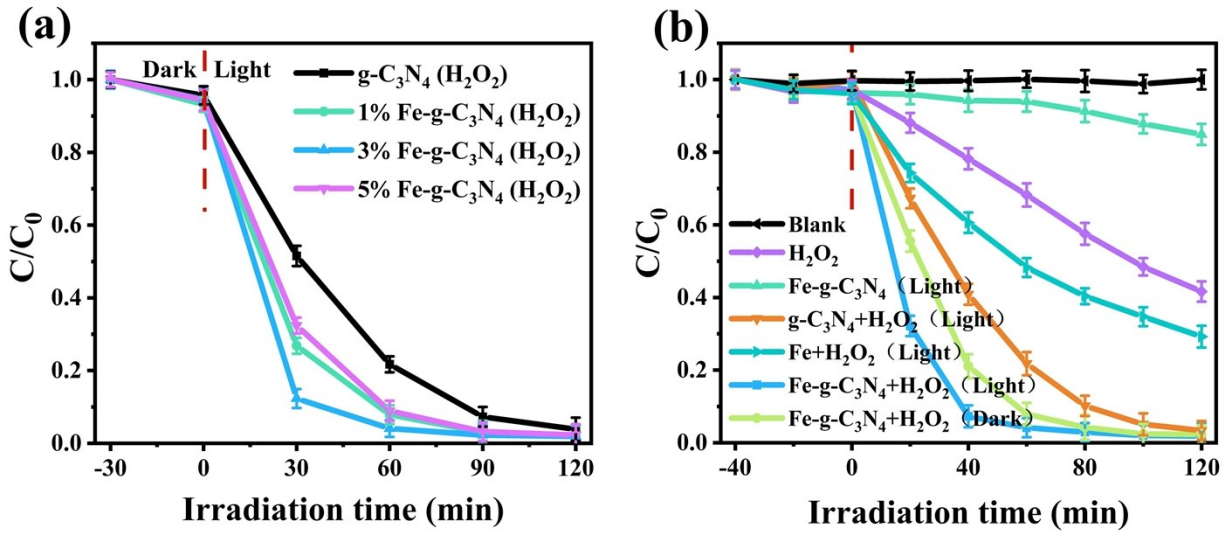

Fig. S1. The Fe-g-C_3N_4 photocatalysis-Fenton system promotes: (a) heterogeneous Fenton reaction and (b) typical photo-Fenton reaction in Rhodamine B (Initial concentration=10mg/L) pollutant removal. Reaction conditions: [H_2O_2] = 5 mM; initial pH = 7.0.

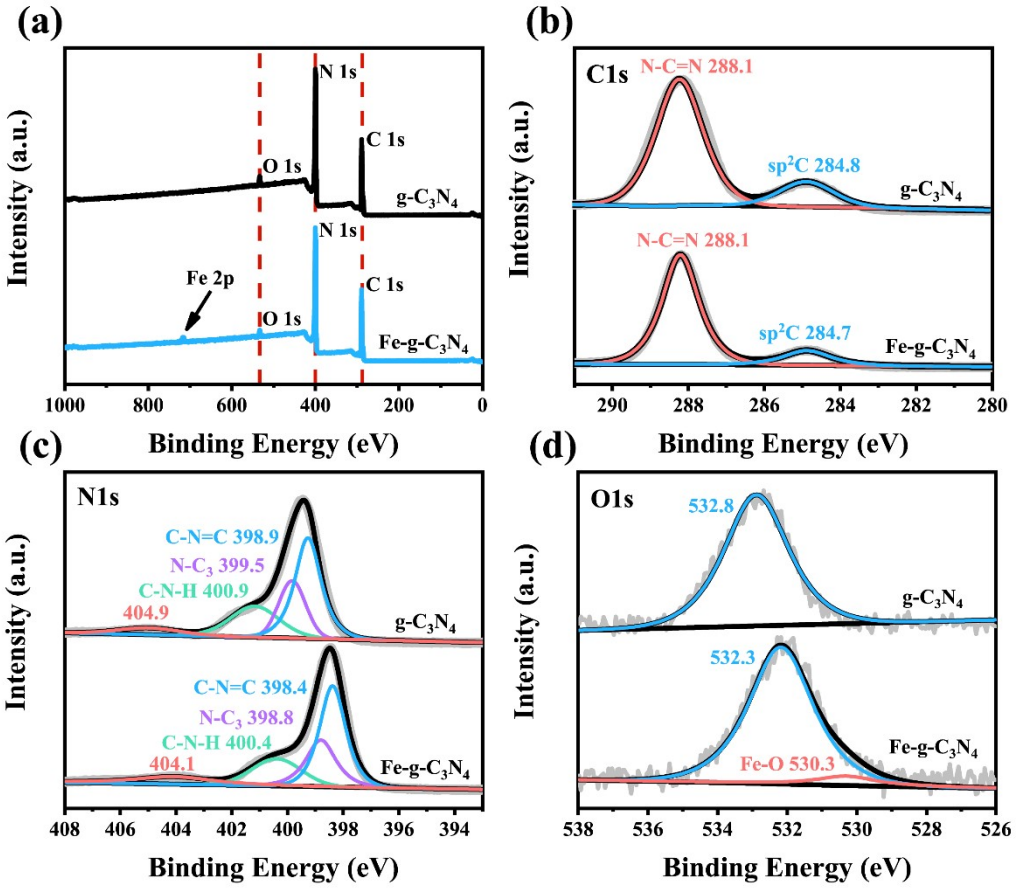

Fig. S2. (a) Survey XPS spectra and high-resolution (d) C 1 s, (e) N 1 s, (f) O 1 s XPS spectra of g-C_3N_4 and Fe-g-C_3N_4.

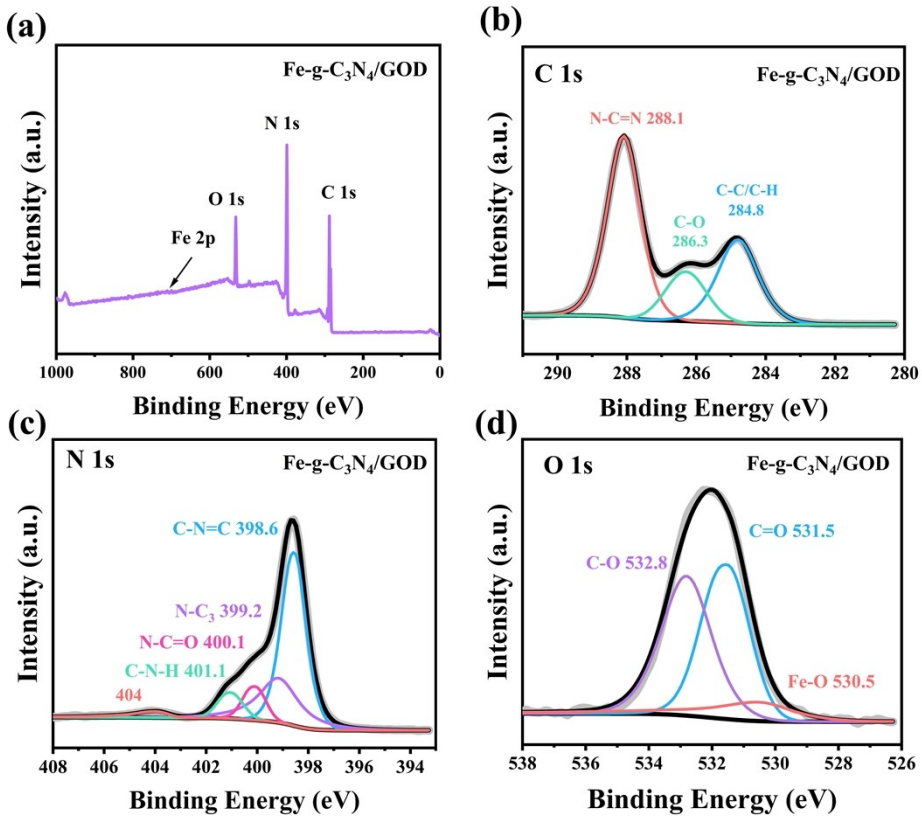

Fig. S3. (a) Survey XPS spectra and high-resolution (d) C 1 s, (e) N 1 s, (f) O 1 s XPS spectra of Fe-g-C_3N_4/GOD.

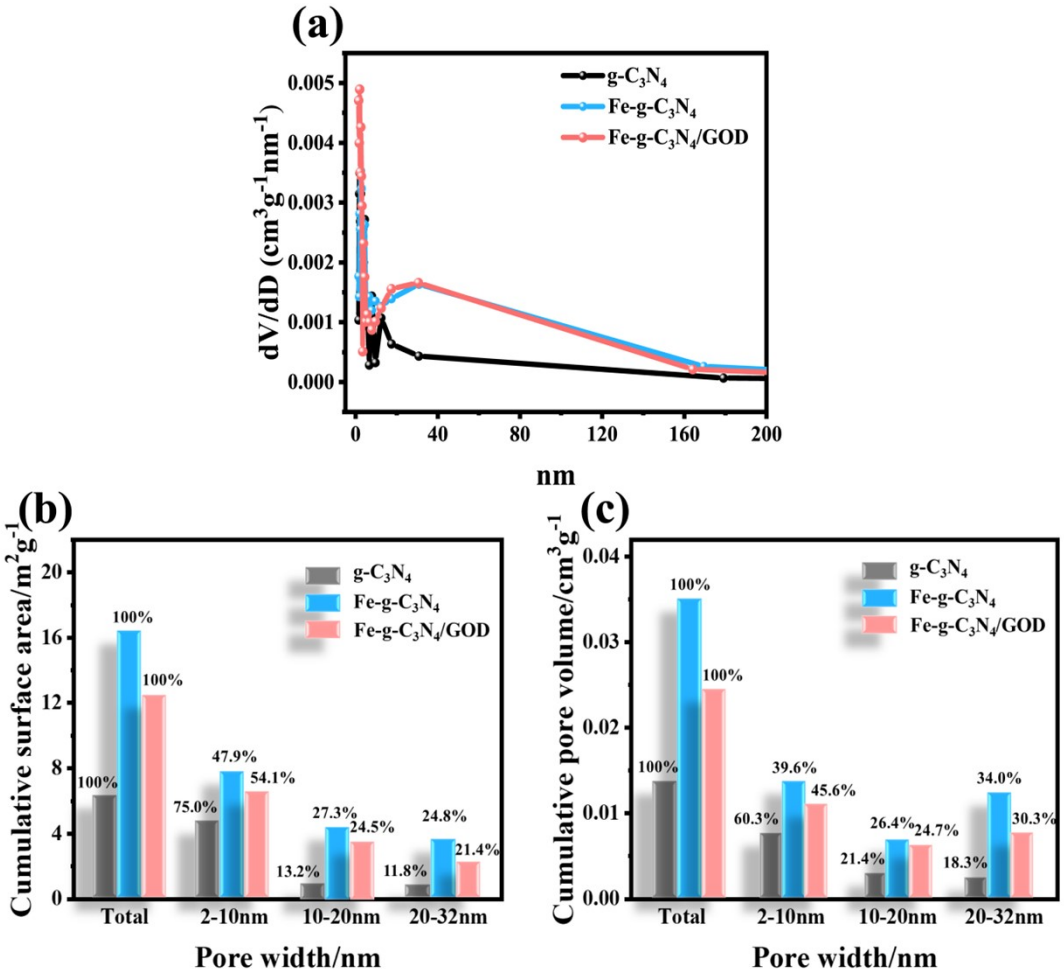

Fig. S4. Specific surface area and pore structure of pure and modified g-C3N4. (a) BJH pore size distributions of g-C_3N_4, Fe-g-C_3N_4 and Fe-g-C_3N_4/GOD. Contribution ratios of cumulative (b) surface area and (c) pore volume of g-C3N4, Fe-g-C_3N_4 and Fe-g-C_3N_4 calculated by the ODFT model.

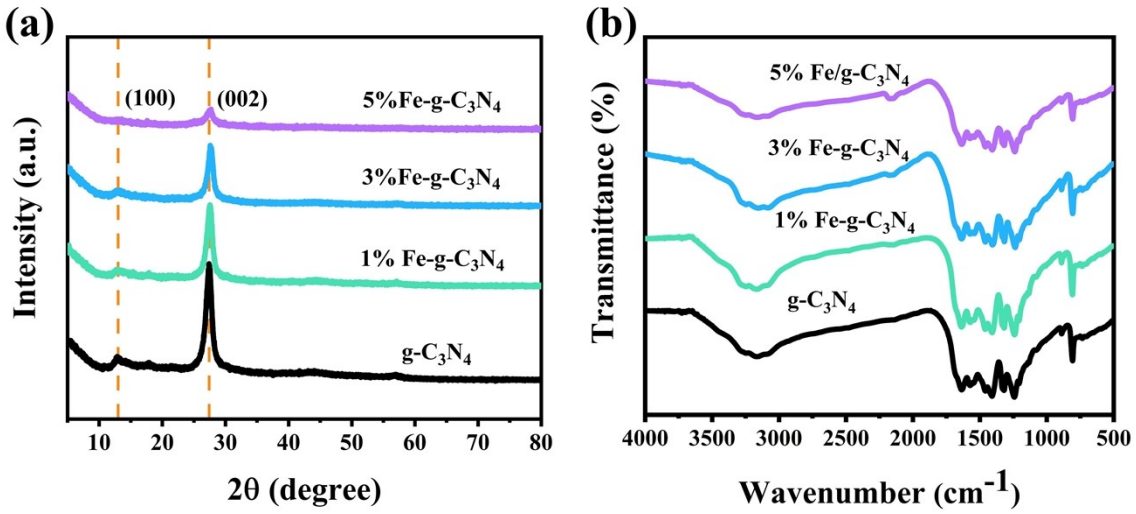

Fig. S5. (a) XRD patterns and (b) FTIR spectra of g-C_3N_4 and x% Fe-g-C_3N_4 samples.

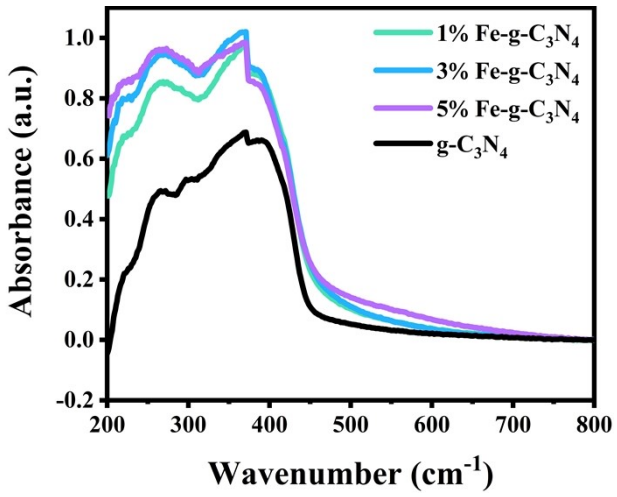

Fig. S6. The UV–vis diffuse reflectance spectra of g-C_3N_4 and x% Fe-g-C_3N_4.

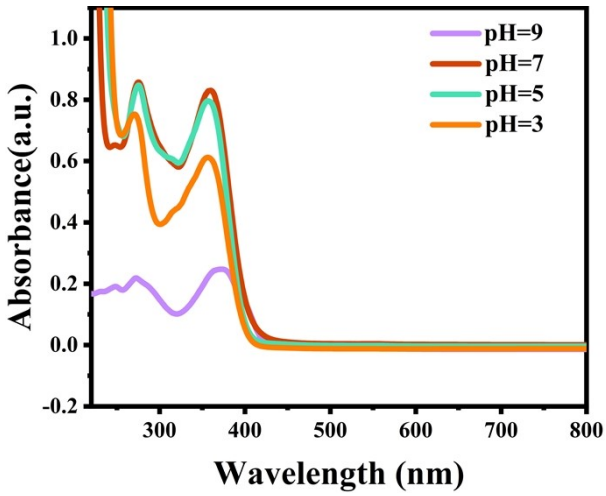

Fig. S7. Influence of pH values on the performance of tetracycline.

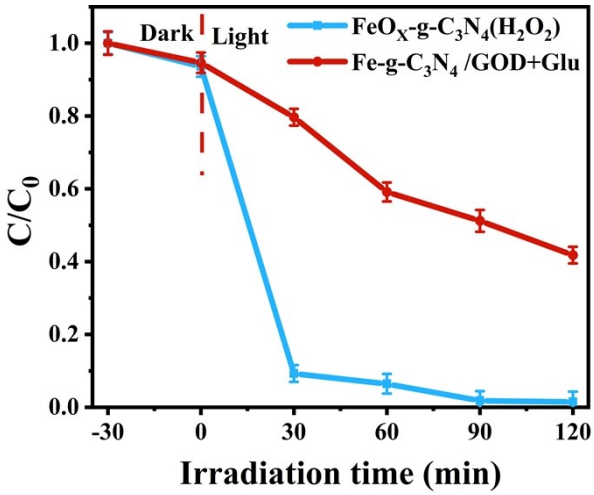

Fig. S8. Comparison of photocatalytic degradation of Rhodamine B over the Fe-g-C_3N_4/GOD+ Glu and the traditional FeO_x-g-C_3N_4/H_2O_2 Fenton-like system.

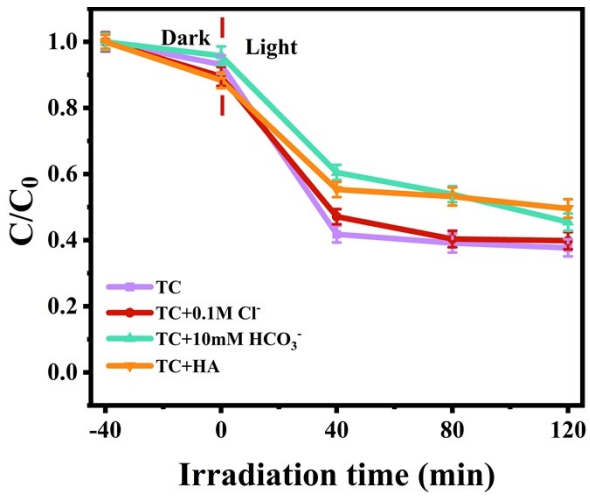

Fig.S9. Influence of Common Interferents in Real Wastewater (0.1 M Cl^-, 10 mM HCO_3^-, 10 mg L^{-1} Humic Acid) on the Photocatalytic Fenton Degradation of Tetracycline (TC).

References

1. W. Shi, C. Zhang, H. Zhao, B. Zhang, H. Tang, Y. Liu and B. Zhang, Water Research, 2024, 266, 122428.
2. D. Zheng, Y. Su, D. Wen, Z. Zhang, P. Yang, X. Ma, Y. Chen, L. Deng, S. Zhou and A. Meng, Journal of Catalysis, 2023, 428, 115180.
3. Y. Liu, Y. Zheng, W. Zhang, Z. Peng, H. Xie, Y. Wang, X. Guo, M. Zhang, R. Li and Y. Huang, Journal of Materials Science & Technology, 2021, 95, 127-135.
4. T. Ge, X. Jin, J. Cao, Z. Chen, Y. Xu, H. Xie, F. Su, X. Li, Q. Lan and L. Ye, Journal of the Taiwan Institute of Chemical Engineers, 2021, 129, 104-111.
5. Y. Chen, X. Yan, J. Xu and L. Wang, Journal of Materials Chemistry A, 2021, 9, 24056-24063.
6. S. Samanta, R. Yadav, A. Kumar, A. Kumar Sinha and R. Srivastava, Applied Catalysis B: Environmental, 2019, 259, 118054.
7. X. Zhang, P. Ma, C. Wang, L. Gan, X. Chen, P. Zhang, Y. Wang, H. Li, L. Wang, X. Zhou and K. Zheng, Energy & Environmental Science, 2022, 15, 830-842.
8. Jiang, L. Wang, J. Lei, Y. Liu and J. Zhang, Applied Catalysis B: Environmental, 2019, 241, 367-374.
9. M. S. Yalfani, S. Contreras, F. Medina and J. Sueiras, Applied Catalysis B: Environmental, 2009, 89, 519-526.
10. Y. Liu, Q. Fan and J. Wang, Journal of Hazardous Materials, 2018, 342, 166-176.
11. X. Liu, J.-H. Fan and L.-M. Ma, Chemical Engineering Journal, 2014, 236, 274-284.
12. M. Li, J. Jiang, Z. Zhu, C. Fang, C. Liu, H. Zhu and Y. Chen, Chemical Engineering Journal, 2025, 509, 161423.
13. S. Yan, Y. Li, X. Yang, X. Jia, J. Xu and H. Song, Advanced Materials, 2024, 36, 2307967.
14. Y. Lin, Z. Feng, P. Li, S.-C. Li, J. Zou, Y. Gui and L. Liu, Chemical Engineering Journal, 2025, 522, 167927.